

## ASPECTS OF ARTERIAL WALL SIMULATIONS: NONLINEAR ANISOTROPIC MATERIAL MODELS AND FLUID STRUCTURE INTERACTION

Daniel Balzani<sup>1</sup>, Simone Deparis<sup>2</sup>, Simon Fausten<sup>1\*</sup>, Davide Forti<sup>2</sup>, Alexander Heinlein<sup>3</sup>, Axel Klawonn<sup>3</sup>, Alfio Quarteroni<sup>2</sup>, Oliver Rheinbach<sup>4</sup>, and Jörg Schröder<sup>1</sup>

<sup>1</sup> Institute of Mechanics, University of Duisburg-Essen, Department of Engineering,  
Universitätsstraße 15, 45141 Essen, Germany,

<sup>2</sup> Chair of Modeling and Scientific Computing, MATHICSE - EPFL, Station 8, 1015 Lausanne,  
Switzerland

<sup>3</sup> Mathematical Institute, University of Cologne, Weyertal 86-90, 50931 Köln, Germany

<sup>4</sup> Institute of Numerical Mathematics and Optimization, TU Bergakademie Freiberg,  
Akademiestraße 6, 09599 Freiberg, Germany

**Key words:** Arterial Walls, Finite Element Method, Nonlinear Solid, Fluid Structure Interaction, Parallel Simulation, Domain Decomposition.

**Abstract.** The simulation of the physiological loading situation of arteries with moderate atherosclerotic plaque may provide additional indicators for medical doctors to estimate if the plaque is likely to rupture and if surgical intervention is required. In particular the transmural stresses are important in this context. They depend strongly on the mechanical response and thus, a predictive material model capturing all characteristics of the material behavior is required. Here, polyconvex strain energy functions are considered for the hyperelastic behavior and a simplified viscoelastic model is proposed which does not take into account an isochoric strain energy for the fiber response. Based thereon, a comparative study is presented, investigating the influence of viscoelasticity on the mechanical behavior of a simplified arterial wall and a rather small impact is found. Realistic predictions of transmural stress distributions require a simulation of the interaction between the blood flow and the vessel wall. We recall the equations that model fluid-structure interaction and the monolithic Convective Explicit algorithm for their numerical approximation, addressing both the cases when the fluid-structure meshes are conforming and nonconforming at the interface. We also present numerical experiments, using the monolithic approach, for the fluid structure interaction problem in a curved tube using a hyperelastic material model for the structure and an absorbing boundary condition. The fluid structure interaction using a highly nonlinear anisotropic structural model for the solid in this context is one of the main contributions of this paper.

## 1 Introduction

Cardiovascular disease is the most frequent cause of death in the industrialized nations. Therefore, the computational simulation of atherosclerotic arteries is of high importance with respect to an optimization of medical treatment. The physiological loading situation of arteries with a moderate atherosclerotic plaque is particularly interesting because here it is often difficult for medical doctors to estimate if the plaque is going to rupture and if surgical intervention is required. A reliable calculation of transmural stress distributions could yield promising further information since concentrations of high stresses are often considered as the main origin of plaque rupture. These stresses depend strongly on the structure and the material behavior of the arterial wall. The mechanical properties are mainly characterized by a nearly incompressible highly nonlinear and anisotropic stress-strain response at finite strains. Furthermore, a viscoelastic behavior is observed in the physiological loading range (i.e. under blood pressure). Various models describing the hyperelastic response of arterial walls by polyconvex energy functions in the sense of [2] have been published throughout the last years, see e.g. [15, 22, 3]. A model that goes beyond the concept of hyperelasticity and includes also an inelastic material behavior is given in e.g. [16]. The approach in [17] takes into account a polyconvex energy function for the hyperelastic response to model the arterial wall as a fiber-reinforced material. Polyconvex energy functions were compared in [4] with their performance in parallel computations using FETI-DP domain decomposition methods. In this contribution a modified approach based on the model in [16] is presented, which also incorporates visco-elasticity by adding a visco-elastic overstress to the second Piola-Kirchhoff stresses. However, the formulation is not restricted to a volumetric-isochoric split of the strain energy function and therefore it allows for stresses induced in the fibers by a volumetric strain. Thereby, an unphysical behavior already observed in [21] for the hyperelastic response is prevented.

Modeling the interaction between the blood flow and the arterial wall represents an important point for a realistic prediction of transmural stress distribution because the vessel deforms under the action of the flow. For a complete overview of the most relevant aspects of the modeling of Fluid-Structure Interaction (FSI) in the context of biomechanics, see [14]. In the context of hemodynamics, the FSI loosely coupled algorithms may lead to instabilities [6], therefore it is essential to devise coupling strategies. The three main ones are segregated algorithms, based on relaxed Picard iterations between the fluid and the structure [20, 13, 19], Steklov-Poincaré formulation on the fluid-structure interface [9], or monolithic where all the variables are grouped into a single system [1, 12, 7]. This work focuses on the latter with a convective explicit time discretization. This approach is well known but applied here using a highly nonlinear, anisotropic structural model.

## 2 Mathematical Model for the Vessel Wall

We consider a physical body in its undeformed reference configuration parameterized in  $\mathbf{X}$  and in its deformed actual configuration parameterized in  $\mathbf{x}$ . The motion of material

points is described by the transformation map  $\varphi_t$  such that the deformation is obtained by  $\mathbf{x} = \varphi_t(\mathbf{X})$ . The deformation gradient and the right Cauchy-Green tensor are defined as  $\mathbf{F} = \nabla\varphi_t(\mathbf{X})$  and  $\mathbf{C} = \mathbf{F}^T\mathbf{F}$ , respectively. For the constitutive framework of the material model we postulate the existence of a strain energy function  $\psi = \psi(\mathbf{C})$  which a priori satisfies the principle of objectivity. The second Piola-Kirchhoff stresses are obtained by  $\mathbf{S} = 2\partial_{\mathbf{C}}\psi(\mathbf{C})$  and can be transformed into the (physical) Cauchy stresses  $\boldsymbol{\sigma} = (\det[\mathbf{F}])^{-1}\mathbf{F}\mathbf{S}\mathbf{F}^T$ ; the Kirchhoff stresses are obtained by  $\boldsymbol{\tau} = \mathbf{F}\mathbf{S}\mathbf{F}^T$ . The introduction of a structural tensor  $\mathbf{M} = \mathbf{a} \otimes \mathbf{a}$  allows the formulation of an isotropic strain energy function  $\psi = \psi(\mathbf{C}, \mathbf{M})$  describing an anisotropic material. Here,  $\mathbf{a}$  denotes the preferred direction of an individual fiber reinforcement. Hence, the strain energy function can be represented with help of the polynomial basis  $P_1 := \{I_1, I_2, I_3, J_4, J_5\}$ , wherein the invariants of the deformation tensor and the additional structural tensor are given by  $I_1 = \text{tr}\mathbf{C}$ ,  $I_2 = \text{tr}[\text{Cof}\mathbf{C}]$ ,  $I_3 = \det\mathbf{C}$ ,  $J_4 = \text{tr}[\mathbf{C}\mathbf{M}]$ ,  $J_5 = \text{tr}[\mathbf{C}^2\mathbf{M}]$ . From a mechanical perspective, soft biological tissues can be considered to be composed of an isotropic ground substance with embedded fibers (collagen and smooth muscle). For arterial walls these fibers are arranged mainly in two directions, winding crosswise helically around the artery. At a material point this may be represented by an isotropic energy function  $\psi^{\text{isot}}$  for the ground substance and the superposition of two transversely isotropic energy functions  $\psi_{(a)}^{\text{ti},\infty}$  for the embedded fibers, cf. [15]. In order to account for the quasi-incompressibility of the material a compression part of the energy  $\psi^{\text{pen}}$  is included as a penalty function. Then the structure of the hyperelastic strain energy function reads

$$\psi(\mathbf{C}, \mathbf{M}_{(1)}, \mathbf{M}_{(2)}) = \psi^{\text{pen}}(I_3) + \psi^{\text{isot}}(I_1, I_3) + \sum_{a=1}^2 \psi_{(a)}^{\text{ti},\infty}(I_1, J_4^{(a)}, J_5^{(a)}). \quad (1)$$

Herein, a specific choice of functional dependency is considered where no dependency on the second invariant is taken into account. Furthermore, the mixed invariants for each fiber family  $\mathbf{a}_{(a)}$  are given by  $J_4^{(a)} = \text{tr}[\mathbf{C}\mathbf{M}_{(a)}]$  and  $J_5^{(a)} = \text{tr}[\mathbf{C}^2\mathbf{M}_{(a)}]$  with the structural tensor  $\mathbf{M}_{(a)} = \mathbf{a}_{(a)} \otimes \mathbf{a}_{(a)}$ . All strain energy functions are chosen to be polyconvex in order to guarantee the existence of minimizers and material stability, cf. [22], [23]. The isotropic and the transversely isotropic contributions to the energy are given by

$$\begin{aligned}
 \psi^{\text{pen}} &= \epsilon_1 (I_3^{\epsilon_2} + I_3^{-\epsilon_2} - 2) \quad \text{and} \quad \psi^{\text{iso}} = c_1 (I_1 I_3^{-1/3} - 3), \\
 \psi_{(a)}^{\text{ti},\infty} &= \alpha_1 \langle I_1 J_4^{(a)} - J_5^{(a)} - 2 \rangle^{\alpha_2},
 \end{aligned} \quad (2)$$

where the restrictions  $c_1 > 0, \epsilon_1 > 0, \epsilon_2 > 1, \epsilon_3 > 1, \alpha_1 > 0$  and  $\alpha_2 > 2$  ensure polyconvexity; the Macaulay brackets are defined as  $\langle (\bullet) \rangle = 1/2(|(\bullet)| + (\bullet))$ . Both parts of the strain energy function are taken from [3]. Note that a volumetric-isochoric split is considered for the isotropic response, but not for the transversely isotropic part since  $\psi_{(a)}^{\text{ti},\infty}$  is not isochoric. In order to extend the material behavior such that a viscoelastic response in the fiber directions can be described an internal variable  $\mathbf{Q}_{\alpha(a)}^{\text{ti}}$ , representing the viscoelastic overstress resulting from the fibers, is introduced on the stress level. Then the second

Piola-Kirchhoff stresses are additively decoupled into a compression part  $\mathbf{S}^{\text{pen}}$ , a part for the isotropic ground substance  $\mathbf{S}^{\text{isot}}$  and a part for the fiber reinforcement which consists of the purely hyperelastic part  $\mathbf{S}_{(a)}^{\text{ti},\infty}$  and  $m$  viscoelastic contributions  $\mathbf{Q}_{\alpha(a)}^{\text{ti}}$ , i.e.

$$\mathbf{S} = \mathbf{S}^{\text{pen}} + \mathbf{S}^{\text{isot}} + \sum_{a=1}^2 \left[ \mathbf{S}_{(a)}^{\text{ti},\infty} + \sum_{\alpha=1}^m \mathbf{Q}_{\alpha(a)}^{\text{ti}} \right]. \quad (3)$$

In this paper, we restrict ourselves to only one viscoelastic relaxation process ( $m = 1$ ) in order to keep the number of additional material parameters small. Note that the stresses  $\mathbf{S}^{\text{pen}}$  do not contain the complete pressure since the transversely isotropic energies are not isochoric. The individual expressions for the stresses are obtained by taking the derivative of the strain energy with respect to the deformation tensor  $\mathbf{C}$ , i.e.  $\mathbf{S}^{\text{pen}} = 2\partial_{\mathbf{C}}\psi^{\text{pen}}$ ,  $\mathbf{S}^{\text{isot}} = 2\partial_{\mathbf{C}}\psi^{\text{isot}}$ , and  $\mathbf{S}_{(a)}^{\text{ti},\infty} = 2\partial_{\mathbf{C}}\psi_{(a)}^{\text{ti},\infty}$ . For the evolution of the overstress we consider the linear differential equation

$$\dot{\mathbf{Q}}_{\alpha(a)}^{\text{ti}} + \frac{\mathbf{Q}_{\alpha(a)}^{\text{ti}}}{\tau_{\alpha}} = \beta_{\alpha}^{\infty} \dot{\mathbf{S}}_{(a)}^{\text{ti},\infty}, \quad (4)$$

which contains additional viscoelastic material parameters, i.e. the relaxation time factor  $\tau_{\alpha}$  and the associated viscoelastic intensity  $\beta_{\alpha}$ . To solve this evolution equation a numerical integration scheme (here the midpoint-rule) is applied and yields the update formula  $\mathbf{Q}_{\alpha(a)}^{\text{ti}} = \mathbf{H}_{\alpha(a)n} + \hat{\mathbf{Q}}_{\alpha(a)}^{\text{ti}}$ , wherein the individual terms are given by

$$\begin{aligned} \mathbf{H}_{\alpha(a)n} &= \exp\left(\frac{-\Delta t}{2\tau_{\alpha}}\right) \left[ \exp\left(\frac{-\Delta t}{2\tau_{\alpha}}\right) \{\mathbf{Q}_{\alpha(a)}^{\text{ti}}\}_n - \beta_{\alpha}^{\infty} \{\mathbf{S}_{(a)}^{\text{ti},\infty}\}_n \right], \\ \hat{\mathbf{Q}}_{\alpha(a)}^{\text{ti}} &= \beta_{\alpha}^{\infty} \exp\left(\frac{-\Delta t}{2\tau_{\alpha}}\right) \mathbf{S}_{(a)}^{\text{ti},\infty}. \end{aligned} \quad (5)$$

Herein,  $\mathbf{H}_{\alpha(a)n}$  represents an expression evaluated at the last time step denoted by  $n$ ;  $\Delta t$  denotes the time increment. Note that we skip the index for the actual time step. The second part of the internal variable  $\hat{\mathbf{Q}}_{\alpha(a)}^{\text{ti}}$  is governed by the hyperelastic transversely isotropic part of the second Piola-Kirchhoff stress. For further information regarding the derivation of the update formulae from the evolution equation the reader is referred to [16] and the references therein.

As an illustration for the model response virtual relaxation tests are performed for different viscoelastic parameters  $\beta_{\alpha}$  and  $\tau_{\alpha}$ . The hyperelastic parameters  $c_1$ ,  $\alpha_1$  and  $\alpha_2$  are taken from [5] where they have been adjusted to experimental data of a media of a human artery. These parameters are given in Table 1. The penalty parameters  $\epsilon_1$  and  $\epsilon_2$  are chosen such that quasi-incompressibility is obtained with  $\det \mathbf{F} = 1 \pm 0.01$ . For the relaxation tests a stretch of  $\lambda = 1.27$  is applied stepwise in one second. Then the displacement is kept constant for 13 further seconds in order to analyze the resulting stress relaxation. The fiber angle (angle between the circumferential and the fiber direction in an arterial wall) is set to  $\bar{\beta}_{\text{f}} = 43^{\circ}$  and the tension direction in the virtual test coincides with the circumferential direction. The results are shown in Figure 1a and illustrate the influence

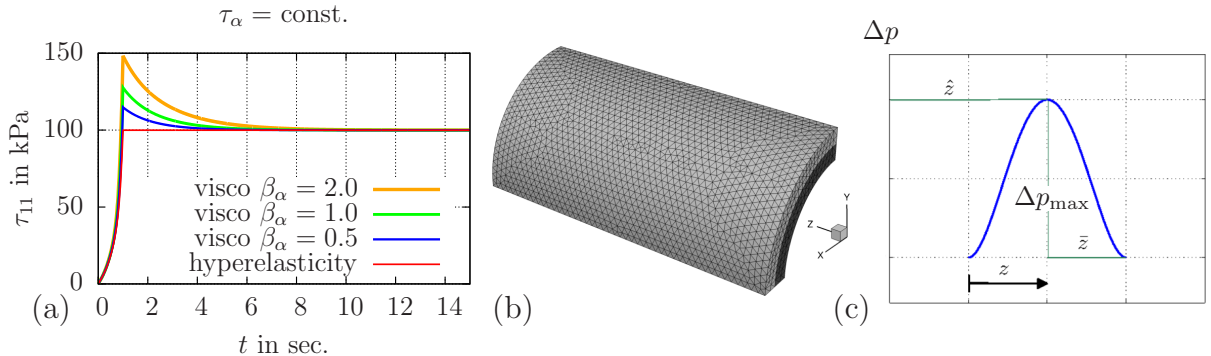
of the viscoelastic intensity parameters  $\beta_\alpha$ . In detail,  $\tau_\alpha = 1.0$  is kept constant and the influence of  $\beta_\alpha$  on the magnitude of the viscoelastic overstress is displayed. Furthermore, the hyperelastic solution is plotted to serve as a reference solution.

### 3 Comparative Study for Viscoelastic Response

In order to analyze the performance of the viscoelastic model the inhomogeneous boundary value problem of an inflated artery is considered. By comparing calculations, where the viscoelastic model and the hyperelastic model are taken into account, we are able to investigate the influence of viscoelasticity on the stress and deformation of an arterial wall. In detail, a thick-walled tube with two layers, media and adventitia, representing an idealized artery, is considered. Due to rotation symmetry only a quarter of the tube is discretized with 28 232 quadratic tetrahedral elements and thus, appropriate symmetry boundary conditions are applied: all nodes with an  $x$ -coordinate equal to zero are fixed in  $x$ -direction, all nodes with a  $y$ -coordinate equal to zero are fixed in  $y$ -direction and all nodes with a  $z$ -coordinate equal to zero are fixed in  $z$ -direction, cf. Figure 1b. This setup allows for an unconstrained expansion of the artery in axial, radial and circumferential direction as a result from an internal pressure. The length of the arterial segment is  $l = 2.0$  cm, the inner radius is 0.5 cm and the two layers have a thickness of 0.1 cm each. In order to obtain a more realistic loading, at first a homogeneous internal pressure of  $p_0 = 80$  mmHg (representing the diastolic blood pressure) is applied stepwise during one second. The resulting situation can be interpreted as a starting configuration for the upcoming simulation, where a distributed pressure  $p(t, z)$  is moved along the artery axis during another second. This reflects a pulse of 120 heart beats per minute. The distributed pressure is illustrated in Fig. 1c and follows the equation

$$p(t, z) = p_0 + \Delta p(t, z) \quad \text{with} \quad \Delta p(t, z) = \Delta p_{\max} \frac{(z + \hat{z})^4}{\bar{z}^4} [(z + \hat{z})^2 - 2\bar{z}^2] - \Delta p_{\max}, \quad (6)$$

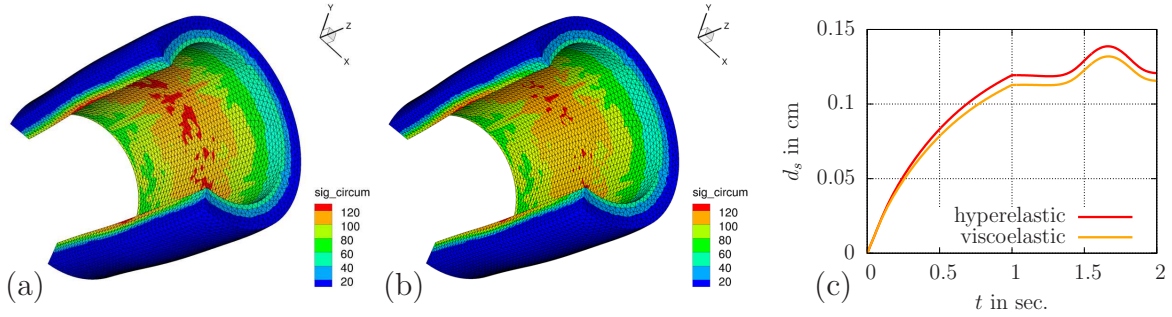
wherein  $\hat{z}(t) = (t - 1) \cdot l - \bar{z}$  denotes the axial coordinate of the center and  $\bar{z} = l/4$  the width of the pressure wave. We assume a systolic pressure of 120 mmHg and thus define



**Figure 1:** (a) Relaxation behavior under uniaxial loading for a variation of  $\beta_\alpha$  for constant  $\tau_\alpha$ , (b) mesh and geometry of the simplified artery and (c) function of the applied internal pressure.

**Table 1:** Summarized material parameters for the comparative study of the viscoelastic response for an idealized arterial segment.

Model	Layer	$c_1$ [kPa]	$\varepsilon_1$ [kPa]	$\varepsilon_2$ [-]	$\alpha_1$ [kPa]	$\alpha_2$ [-]	$\tau_\alpha$ [s]	$\beta_\alpha$ [-]
hyperelastic	adventitia	6.6	23.9	10.0	1503.0	6.3	-	-
	media	17.5	499.8	2.4	30001.9	5.1	-	-
viscoelastic	adventitia	6.6	23.9	10.0	1503.0	6.3	1.0	2.0
	media	17.5	499.8	2.4	30001.9	5.1	1.0	2.0

**Figure 2:** Distribution of circumferential Kirchhoff stresses in kPa in the deformed configuration at  $t = 1.64$  seconds for the (a) hyper- and (b) viscoelastic model, and (c) a characteristic displacement  $d_s$  located at the point  $P = (0.5, 0.0, 1.0)$  versus time.

$\Delta p_{\max} = 40\text{mmHg}$ . For this boundary value problem the hyperelastic polyconvex strain energy function introduced above is used. For the two layers of the thick-walled tube material parameters are taken into account which were adjusted to experimental data of the media and adventitia of a human artery, cf. [5]. Due to a lack of experimental data for the viscoelastic material behavior we chose the parameters from the virtual uniaxial relaxation test that showed the maximal overstress out of the selected parameters. All material parameters are summarized in Table 1.

For an interpretation of the results the distribution of the circumferential Kirchhoff stresses for the situation at  $t = 1.64$  seconds, i.e. where the peak of the moving distributed pressure reaches the half of the artery length, is depicted in Figure 2a,b. The results are given for the case where the hyper- (Fig. 2a) and viscoelastic (Fig. 2b) model is considered. There, the deformed configuration is plotted, however, one quarter of the artery is not visualized in order to enable an analysis of the inner stress distribution. It can be clearly seen that the difference between hyper and viscoelasticity is rather small. In order to also analyze a deformation quantity the radial displacement  $d_s$  at the point  $P = (x = 0.5, y = 0.0, z = 1.0)$ , i.e. at the inner side and at the center of the artery length, is plotted versus time in Figure 2c. Interestingly, it can be seen that the difference is not significant. This yields the conclusion that for the given boundary value problem,

considering the given set of parameters, the viscoelastic effect plays a minor role with regard to the material behavior. However, it is emphasized that the incorporation of e.g. residual stresses may lead to a more pronounced difference. This is left to future studies.

#### 4 Fluid Structure Interaction Model

In this Section we briefly introduce the equations adopted to model the fluid structure interaction problem. Let  $\Omega^f$  and  $\Omega^s$  be the fluid and the structure domains, respectively, in their reference configuration. We denote by  $\Gamma = \partial\Omega^f \cap \partial\Omega^s$  the fluid-structure interface. The current fluid domain configuration  $\Omega_f^t$  is given by the Arbitrary Lagrangian Eulerian (ALE) mapping  $\mathcal{A}_t : \Omega_f \rightarrow \Omega_f^t$

$$\mathbf{x} \mapsto \mathcal{A}^t(\mathbf{x}) = \mathbf{x} + \mathbf{d}_f(\mathbf{x}), \quad (7)$$

where  $\mathbf{d}_f$  represents the displacement of the fluid domain. We model the fluid flow using the Navier-Stokes equation written in the ALE frame of reference. The fully coupled fluid-structure interaction problem reads: find the fluid velocity  $\mathbf{u}(\mathbf{x}, t) : \Omega_f \times \mathbb{R}^+ \rightarrow \mathbb{R}^3$ , the pressure  $p(\mathbf{x}, t) : \Omega_f \times \mathbb{R}^+ \rightarrow \mathbb{R}$  and the displacement of the structure  $\mathbf{d}_s(\mathbf{x}, t) : \Omega_s \times \mathbb{R}^+ \rightarrow \mathbb{R}^3$  such that:

$$\begin{cases} \rho_f \partial_t \mathbf{u}|_{\mathcal{A}} + \rho_f (\mathbf{u} - \mathbf{w}) \cdot \nabla \mathbf{u} - \nabla \cdot \boldsymbol{\sigma}_f = 0 & \text{in } \Omega_f^t, \\ \nabla \cdot \mathbf{u} = 0 & \text{in } \Omega_f^t, \\ \rho_s \partial_{tt} \mathbf{d}_s - \nabla \cdot (\mathbf{FS}) = 0 & \text{in } \Omega_s, \end{cases} \quad (8)$$

with the following fluid-structure coupling conditions:

$$\begin{cases} \mathbf{d}_f = \text{Ext}(\mathbf{d}_s|_{\Gamma}), \mathbf{w} = \partial_t \mathbf{d}_f & \text{in } \Omega_f, \\ \mathbf{u} = \partial_t \mathbf{d}_s & \text{on } \Gamma, \\ \boldsymbol{\sigma}_f \mathbf{n}_f + (\mathbf{FS}) \mathbf{n}_s = 0 & \text{on } \Gamma. \end{cases} \quad (9)$$

In (8)  $\rho_f$  and  $\rho_s$  are the density of the fluid and the structure, respectively,  $\mathbf{w}$  is the fluid mesh velocity,  $\boldsymbol{\sigma}_f$  is the Cauchy fluid stress tensor,  $\mathbf{FS}$  are the first Piola-Kirchhoff stresses,  $\mathbf{n}_f$  and  $\mathbf{n}_s$  are the outward unit normals to the fluid and the structure domains. In (9), we denoted by  $\text{Ext}(\cdot)$  the extension operator that defines  $\mathbf{d}_f$  as the harmonic extension of  $\mathbf{d}_s|_{\Gamma}$  to the interior of the fluid reference domain  $\Omega_f$ .

#### 5 Monolithic Algorithm and Nonconforming Meshes for FSI

We use a Convective Explicit scheme (CE) [7] for the time discretization of the FSI problem and the finite element method for the discretization in space. The fully coupled

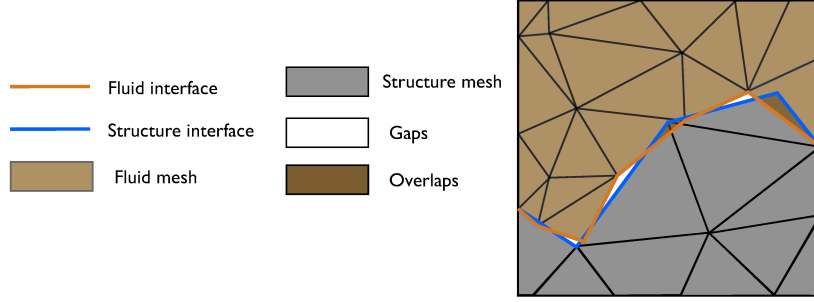


**Figure 3:** Presence of gaps and overlaps across interface.

discretized FSI system reads:

$$\begin{pmatrix} F_{ff} & F_{f\Gamma} & 0 & 0 & 0 & 0 & 0 \\ F_{\Gamma f} & F_{\Gamma\Gamma} & 0 & 0 & \Phi_{sf} & 0 & 0 \\ \hline 0 & 0 & S_{ss} & S_{s\Gamma} & 0 & 0 & 0 \\ 0 & 0 & S_{\Gamma s} & S_{\Gamma\Gamma} & -I & 0 & 0 \\ \hline 0 & \Phi_{fs} & 0 & -I/\Delta t & 0 & 0 & 0 \\ \hline 0 & 0 & 0 & 0 & 0 & H_{ff} & H_{f\Gamma} \\ 0 & 0 & 0 & -\Phi_{sf} & 0 & 0 & I \end{pmatrix} \begin{pmatrix} (\mathbf{u}_f, p)^{n+1} \\ (\mathbf{u}_f, p)_{\Gamma}^{n+1} \\ \mathbf{d}_s^{n+1} \\ \mathbf{d}_{s\Gamma}^{n+1} \\ \boldsymbol{\lambda}^{n+1} \\ \mathbf{d}_f^{n+1} \\ \mathbf{d}_{f\Gamma}^{n+1} \end{pmatrix} = \begin{pmatrix} \mathbf{b}_f \\ \mathbf{b}_{f\Gamma} \\ \mathbf{b}_s \\ \mathbf{b}_{s\Gamma} \\ -\mathbf{I}/\Delta t \mathbf{d}_{s\Gamma}^{n+1} \\ 0 \\ 0 \end{pmatrix} \quad (10)$$

where  $\boldsymbol{\lambda}$  are the Lagrange multipliers that enforce the stress balance across  $\Gamma$ ,  $F_{ij}$  and  $S_{ij}$  (with  $i, j = f, s$  or  $\Gamma$ ) correspond to the sub-blocks of the finite element matrices of the fluid and the structure, respectively. Here,  $\Phi_{fs}$ , and  $\Phi_{sf}$  are identity matrices which allow for the transfer of data between the fluid and the structure at the interface.

In the numerical simulation of fluid-structure interaction problems, it is sometimes desirable to have nonconforming meshes at the interface between the fluid-structure domains because the cost of producing conforming meshes may be prohibitive and, in addition, because of the different mesh requirements for the fluid and structure. The use of nonconforming meshes may imply that at the discrete interface between the domains there can be gaps and/or overlaps between the meshes or even the geometries, as it is illustrated in Figure 3.

System (10) is written for conforming fluid-structure meshes at the interface, we have therefore to reformulate it. When the meshes are nonconforming, an interpolation procedure has to be introduced to transfer physical quantities from the fluid to the structure interface,  $\Phi_{fs}$ , and vice versa,  $\Phi_{sf}$ . Dealing with nonconforming meshes,  $\Phi_{fs}$  and  $\Phi_{sf}$  are rectangular matrices with  $\Phi_{fs} \in \mathbb{R}^{n_{s\Gamma} \times n_{f\Gamma}}$  and  $\Phi_{sf} \in \mathbb{R}^{n_{f\Gamma} \times n_{s\Gamma}}$ , being  $n_{f\Gamma}$  and  $n_{s\Gamma}$  the number of degrees of freedom at the fluid and structure interfaces, respectively. In this work we use the Rescaled Localized Radial Basis Function (RL-RBF) interpolation proposed in [10] to build the operators  $\Phi_{fs}$  and  $\Phi_{sf}$ .

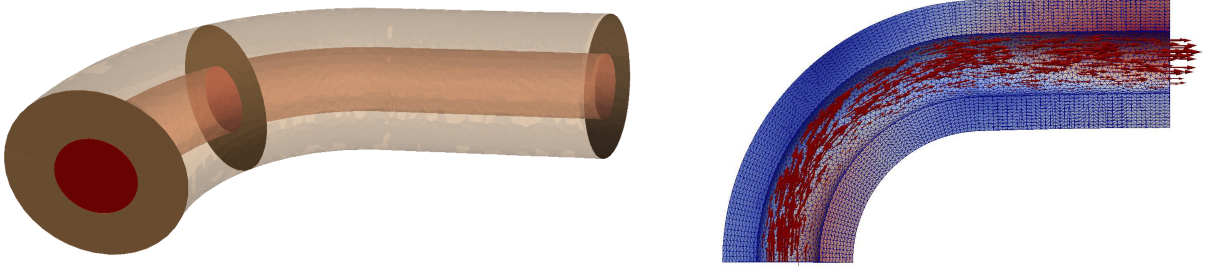


**Figure 4:** Geometry of the FSI problem (left): 1 cm radius of the centerline of the curved part, 1 cm length of the straight part, 0.33 cm outer radius of the structure, 0.15 cm inner radius of the structure. Mesh #5 cut open (right): Color represents the displacement of the structure at time 0.03s.

## 6 Numerical Experiments on Fluid Structure Interaction

In our experiments, we consider the fluid structure interaction of fluid flow in a curved tube; see Figure 4 for the geometry and the dimensions. The geometry consists of a curved and a straight section and can be seen as an idealized coronary artery. The tube is composed of a single material, i.e., we use the nonlinear hyperelastic material model in (1) and the corresponding parameters for the media from Table 1. The fiber angle is set to  $\bar{\beta}_f = 43^\circ$ . We use P1-P1 finite elements for the fluid (stabilized by interior penalty) and P1 elements for the structure.

We solve the monolithic system (10) containing the fluid, the solid and the geometry problem. Here, for the fluid we use a Convective Explicit (CE) time discretization, i.e., the convective term is treated explicitly; for details, see [7, 8]; for simplicity we also use matching fluid and structure nodes. We use the LifeV software library 3.6.2 [18] coupled to the Finite Element Analysis Program (FEAP 8.2) [25] using a lightweight coupling library [11].

The displacement of the structure is fixed in axial direction at the faces at both ends of the tube. Absorbing boundary conditions are imposed at the outlet according to [20] in order to reduce wave reflections at the outlet. Combining the Dirichlet boundary conditions and the (Robin-type) absorbing boundary condition we obtain a statically determined structure. Note that these absorbing boundary conditions assume a linear elastic structural model. In our nonlinear setting, in general, we therefore cannot expect these boundary conditions to remove reflections completely.

For the fluid, we use a parabolic inflow velocity profile. The peak value is defined according to  $v(t) = \frac{t}{T_R} v_{steady}$  for  $0 \leq t \leq T_R$ , and  $v(t) = v_{steady}$  for  $T_R \leq t \leq T_F$ , i.e., it is increased linearly on  $0 \leq t \leq T_R$  until  $v_{steady}$  is reached. Here,  $T_R = 0.0177$ s and  $v_{steady} = 177$  cm/s,  $T_F = 0.1$  s. The inflow boundary conditions are intended to lead to a pressure of 80mmHg at a steady state for the coarsest mesh.

The time advancing method used in the simulations is a BDF scheme of second order with  $\Delta t = 0.0001$ . We will use the composed Dirichlet-Neumann preconditioner, see [7], using a parallel one-level algebraic additive Schwarz preconditioner [24] on each of

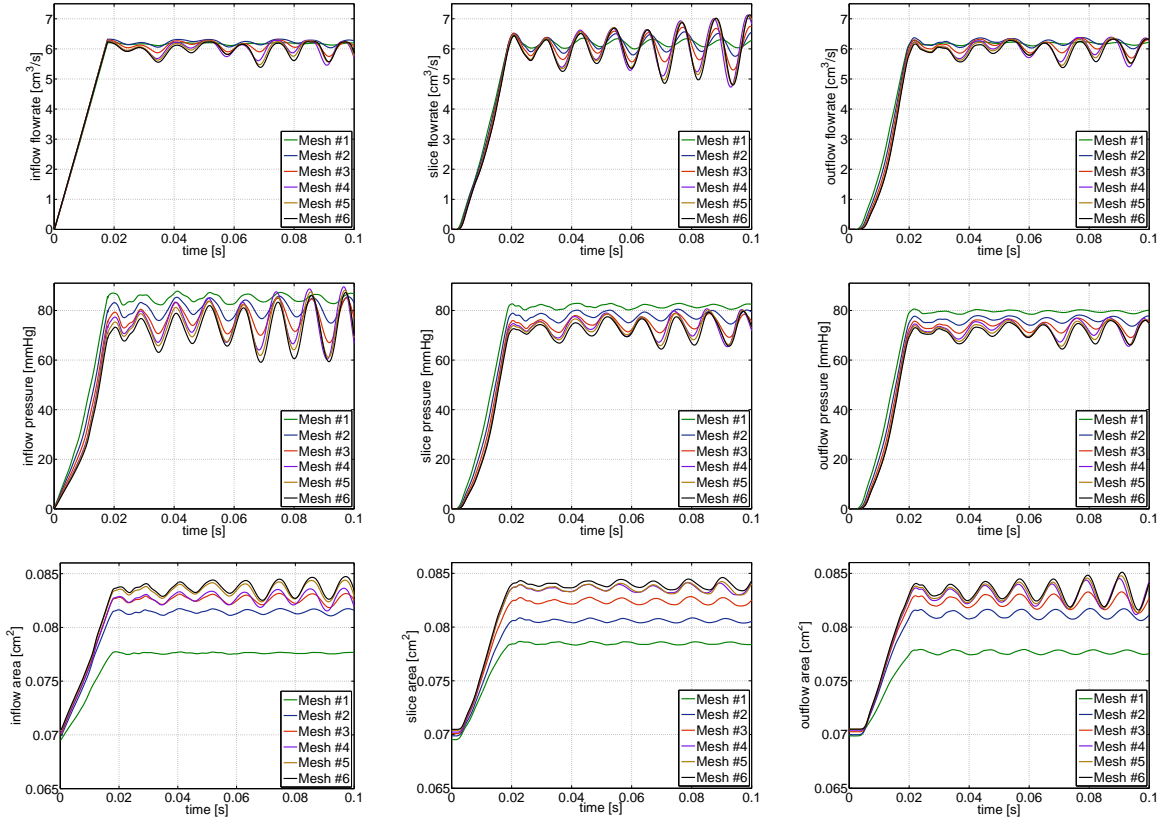


**Figure 5:** Flowrate (top), average pressure (middle) and lumen cross section area (bottom) over time at the inlet (left), slice (middle), and outlet (right).

the blocks of the Dirichlet-Neumann preconditioner. We used 6 different meshes containing  $4\,856+1\,785$  (solid+fluid),  $9\,264+2\,269$ ,  $19\,008+3\,506$ ,  $33\,605+5\,045$ ,  $51\,018+9\,373$ , and  $93\,847+16\,247$  nodes. The results are shown in Figure 5. The leftmost plots always correspond to the inlet, the rightmost to the outlet of the tube. The center plot corresponds to values at the slice in the curved section of the tube, cf. Figure 4. Our results seem to indicate mesh convergence although we clearly observe oscillations, and no steady state is reached in our computations. It is necessary to investigate these oscillations in more detail in the future. They may result from remaining wave reflections at the outflow since the absorbing boundary conditions are not designed for our nonlinear setting. Using a smooth function for the inflow, instead of the function used here, may also help.

## 7 Conclusion and Outlook

A viscoelastic model was proposed combining the approach in [16] with polyconvex strain energy functions for the fibers in soft biological tissues which are not assumed to be isochoric. A parameter study performed for a relaxation test showed the impact of

the parameters on the resulting material behavior. The parameters, for which a strong viscoelastic effect was observed at the material point, were used in a numerical study to analyze the influence of viscoelasticity in an artery under blood pressure. Interestingly, it turned out that the influence is rather small. In this first result neither wall shear stresses stemming from fluid-structure interaction nor residual stresses in the wall were taken into account, which are however expected to have a significant influence. In the next step a biologically motivated model is planned to be included in the wall model and its influence on the overall behavior is to be investigated.

In our fluid structure interaction problem using the hyperelastic structural model we observe that no steady state is reached as a result of oscillations. These may be due to remaining wave reflections at the absorbing boundary condition which was developed for a linear elastic structure. These phenomena have to be investigated in more detail in the future. Clearly, in the future, the properties of the different layers present in arteries as well as viscoelastic effects should also be accounted for in the fluid structure interaction problem and finite elements of higher order should be used.

## 8 Acknowledgement

Financial support by the German Science Foundation (DFG), project no. KL2094/3-1 and SCHR570/15-1, and the Swiss National Foundation (SNF), project no. 140184 is gratefully appreciated. Alexander Heinlein, Axel Klawonn, and Oliver Rheinbach acknowledge the use of the CHEOPS cluster at the University of Cologne and the Cray XT6m at the University of Duisburg-Essen.

## REFERENCES

- [1] S. Badia, A. Quaini, A. Quarteroni. Splitting methods based on algebraic factorization for fluid-structure interaction. *SIAM J. Sci. Comput.*, **30(4)**, 1778–1805, 2008.
- [2] J.M. Ball. Convexity conditions and existence theorems in non-linear elasticity. *Arch. Ration. Mech. Anal.*, **63**, 337–403, 1977.
- [3] D. Balzani, P. Neff, J. Schröder and G.A. Holzapfel. A polyconvex framework for soft biological tissues. adjustment to experimental data. *IJSS*, **43(20)**, 6052–6070, 2006.
- [4] D. Balzani, D. Böse, D. Brands, R. Erbel, A. Klawonn, O. Rheinbach, J. Schröder. Parallel Simulation of Patient-specific Atherosclerotic Arteries for the Enhancement of Intravascular Ultrasound Diagnostics. *Engineering Computations*, **29(8)**, 2012.
- [5] D. Brands, A. Klawonn, O. Rheinbach, J. Schröder. Modelling and Convergence in Arterial Wall Simulations Using a Parallel FETI Solution Strategy. *Comp. Meth. Biomech. Biomed. Engrg.*, **11(5)**, 1476–8259, 2008.
- [6] P. Causin, J. F. Gerbeau, and F. Nobile. Added-mass effect in the design of partitioned algorithms for fluid-structure problems. *CMAME*, **194**:4506–4527, 2005.
- [7] P. Crosetto, S. Deparis, G. Fourestey, and A. Quarteroni. Parallel algorithms for fluid-structure interaction problems in haemodynamics. *SISC*, **33(4)**, 1598–1622, 2011.

- [8] P. Crosetto, P. Reymond, S. Deparis, D. Kontaxakis, N. Stergiopoulos, and A. Quarteroni. Fluid Structure Interaction Simulations of Physiological Blood Flow in the Aorta. *Computers and Fluids*, **43(1)**, 46-57, 2011.
- [9] S. Deparis, M. Discacciati, G. Fourestey and A. Quarteroni. Fluid-structure algorithms based on Steklov-Poincaré operators. *CMAME*, **195**, 5797–5812, 2006.
- [10] S. Deparis, D. Forti, and A. Quarteroni. A rescaled localized radial basis functions interpolation on non-cartesian and non-conforming grids. *Submitted*, 2014.
- [11] A. Fischle, A. Heinlein, A. Klawonn, O. Rheinbach. Coupling library for LifeV and FEAP. *Unpublished*, 2014.
- [12] M.W. Gee, U. Küttler, and W.A. Wall. Truly Monolithic Algebraic Multigrid for Fluid-Structure Interaction. *Int. J. Num. Meth. Engrg.*, **85**, 987–1016, 2011.
- [13] J.F. Gerbeau, M. Vidrascu. A quasi-Newton algorithm based on a reduced model for fluid-structure interaction problems in blood flows. *Mathematical Modelling Numerical Analysis*, **37(4)**, 631–648, 2008.
- [14] L. Formaggia, A. Quarteroni, and A. Veneziani. *Cardiovascular Mathematics*. MS&A: Modeling, Simulation and Applications. Springer, Heidelberg, 2009.
- [15] G.A. Holzapfel, T.C. Gasser and R.W. Ogden. A new constitutive framework for arterial wall mechanics and a comparative study of material models. *Jour. Elast.*, **61**, 1–48, 2000.
- [16] G.A. Holzapfel and T. Gasser. A viscoelastic model for fiber-reinforced composites at finite strains. Continuum basis, computational aspects and applications. *CMAME*, **190**, 4379–4403, 2001.
- [17] M. Itskov, A.E. Ehret. A Universal Model for the Elastic, Inelastic and Active Behaviour of Soft Biological Tissues. *GAMM-Mitteilungen*, **32(2)**, 221-236, 2009.
- [18] LifeV webpage: <http://www.lifev.org>.
- [19] H.G. Matthies and J. Steindorf. Partitioned strong coupling algorithms for fluid-structure interaction. *Computers & Structures*, **81(8)**, 805–812, 2003.
- [20] F. Nobile and C. Vergara. An effective fluid-structure interaction formulation for vascular dynamics by generalized Robin conditions. *SISC*, **30(2)**:731–763, 2008.
- [21] C. Sansour. On the physical assumptions underlying the volumetric-isochoric split and the case of anisotropy. *European Journal of Mechanics A/Solids*, **27**, 28–39, 2008.
- [22] J. Schröder, P. Neff. Invariant formulation of hyperelastic transverse isotropy based on polyconvex free energy functions. *Int. J. Solids Struct.*, **40**, 401–45, 2003.
- [23] J. Schröder, P. Neff, and D. Balzani. A Variational Approach for Materially Stable Anisotropic Hyperelasticity. *Int. J. Solids Struct.*, **42/15**, 4352–4371, 2005.
- [24] B. F. Smith, P. E. Bjørstad, W. D. Gropp. 1996. Domain Decomposition: Parallel Multilevel Methods for Elliptic Partial Differential Equations. *Cambridge Univ. Press*, NY, USA.
- [25] R. L. Taylor. FEAP webpage: <http://www.ce.berkeley.edu/projects/feap>.